

CONCRETE FILLED STEEL TUBULAR COLUMNS, A FINITE ELEMENT STUDY

By Aaron W. Malone

University of Massachusetts Amherst

Department of Civil and
Environmental Engineering
236 Marston Hall
Amherst, MA 10003
(413) 577-0142

ABSTRACT

This study focuses on the behavior of concrete-filled tubular (CFT) columns under combined axial load and bending moment. The study was conducted using ANSYS finite element software. Both stub columns and slender columns were studied with varying amounts of load eccentricity; tests were run for both hollow tubes and CFTs. Results were compared to study buckling failure modes and section capacities. The results showed that local buckling governed for stub columns while global buckling controlled for the slender columns. Comparison of hollow and CFT tubes showed that the concrete core delayed the onset of local buckling of the steel tube.

INTRODUCTION

CFT columns have the potential of becoming commonplace structural members in both low-rise and high-rise building construction. The advantages of using CFT columns in structures are: economic designs, improved constructability, and enhanced performance. CFT columns are constructed by erecting hollow steel columns as a structure's frame which are then filled with concrete as construction advances. The use of CFT columns in construction offers several major economic advantages over steel or reinforced concrete columns; since the steel tube serves as formwork and confinement for the concrete, the material and labor costs associated with formwork and steel reinforcement are eliminated. CFTs also allow steelwork to precede several stories above concrete pouring, which reduces construction time and improves the coordination of steel and concrete trades.

The composite action of steel and concrete is what gives CFT columns their advantages over standard steel or reinforced concrete columns. The concrete core can act to increase the stiffness and compressive strength of the hollow steel tube and to delay local buckling. The hollow steel tube acts as concrete reinforcement, resists bending moments and shear forces, and confines the concrete thereby increasing ductility. These potential benefits of composite action depend largely on the bond at the steel-concrete interface. Unfortunately the transfer of stress through the interface bond is not well understood. The

use of these systems and the development of design guidelines are hampered by a lack this lack of information.

In the United States typical beam to column connections to CFTs consist of a gusset plate welded to the steel tube, which transfers beam loading to the steel tube. Since the gusset plate attaches only to the steel tube, the bond at the steel-concrete interface must transfer a shear force to the concrete core in order for composite action to be effective. Limited research has been conducted on the effect of varying the method of load application to the CFT at the connection to show the effect of also loading the concrete section at the connection. Several studies have suggested that the inherent bending in a column can improve the stress transfer at the interface thus allowing some composite action. The extreme difficulty of measuring the stress distribution at the bond interface limits the understanding gained by experimental research. Finite element analysis would allow the stress demand at the interface to be analyzed in greater detail than is possible in the laboratory.

The scope of this study was to develop finite element models that accurately predict accepted theoretical capacities of hollow and concrete filled tubular columns. The analysis results were analyzed to determine the modes of failure and the effect of the concrete core on the steel tube. For the scope of this study perfect bonding was assumed at the concrete-steel interface. The models developed in this study will be modified in future research to look specifically at the bond behavior at the steel-concrete interface. The results of this study will supplement experimental research being conducted at the University of Massachusetts Structural Engineering Laboratory.

TEST PROGRAM

Specimen Geometry

All modeling was conducted using ANSYS 5.7 finite element software. The project proceeded in several stages of modeling; all specimens were modeled as 3D solid objects with identical geometry. The dimensions of the sections were chosen to match those being used in the experimental testing of

the author's thesis project. A total of 12 specimens were tested for this study. Four separate models were developed and tested for this project, a stub column and slender column were developed of a hollow tube section and a CFT section. Figure 1 shows the geometry of the sections modeled.

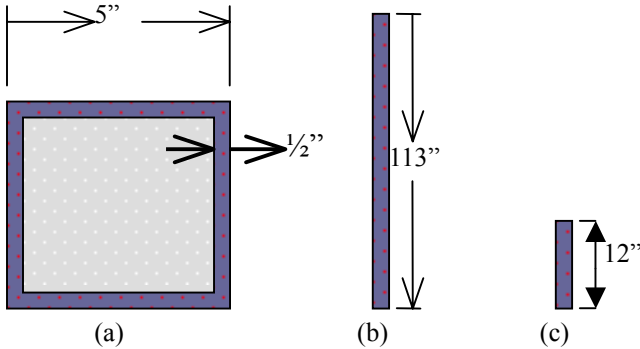


Figure 1: Specimen Geometry: (a) cross-section, (b) slender columns, (c) stub columns

Loading and Constraints

Each of the four specimens was tested with eccentricities of 0-inch, 1-inch, and 2-inch. Loads were applied as concentrated loads to a 2-inch thick plate that was rigidly attached to the ends of the column and bears on the entire cross-section. The end plates were assumed to be ASTM Gr50 steel. Boundary constraints consisted of hinges at each end plate which allowed rotation of the specimen in the plane of bending caused by the eccentricity. One hinge was released to allow vertical deformation of the tube during loading. Figure 2 shows a schematic of the loading condition at the ends of each tube.

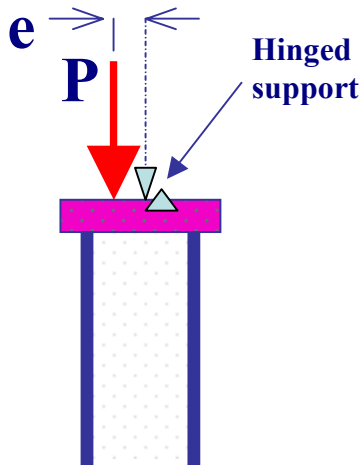


Figure 2: Loading Geometry

Modeling Procedure

All specimens were modeled as 3D solid objects using solid structural elements. The element SOLID 45 was used to model the steel tube and the endplates. Steel was assumed to be elastic plastically perfect with $F_y = 50$ -ksi with an elastic modulus $E = 30,000$ -ksi. The element SOLIC 65 was used to model the concrete core of the columns. SOLID 65 supports the cracking and crushing properties of concrete as well as material nonlinearity. This element also accounts for the difference in tensile and compressive strengths of steel. Concrete compressive strength was taken as $f'_c = 3.5$ -ksi, and the tensile strength $f_t = 0.35$ -ksi.

The large deformation effects and stress stiffening options were used for the hollow tube models only. These functions were not used for models involving SOLID 65, as suggested by ANSYS literature. All runs were conducted using the automatic time stepping option.

TEST RESULTS

Hollow Tube Sections

The results for the 6 hollow section tests are summarized in Table 1. This table also includes the plastic section capacities calculated using theory. These results have also been provided in Figure 3. All tests show close agreement with the theoretically calculated value; the largest variance between experimental and expected capacity is 8%. The results also verify that increasing the eccentricity of the load decreases the capacity of the column. Comparison of capacities shows that indeed the slender columns carried less load than stub columns.

Table 1: Hollow Tube Results

e (in)	Hollow Stubs		Hollow Column	
	Theory	ANSYS	Theory	ANSYS
0	168	153	139	135
1	107	116	85	90
2	79	80	64	68

Inspection of the deflected shapes and stress distributions at failure it can be seen that the concentric stub columns failed by yielding of the cross-section, while the two stub columns loaded eccentrically failed by local buckling of the tube wall. Figure 4 shows the deflected shape of the stub column for 2-in eccentricity. Inspection of the deflected shape shows that the tube wall has crimped close to the loading plate. This result can be verified from experimental results of a similar hollow stub column, which also experienced local buckling of the steel tube close to the loading plate.

The results for the CFT test are summarized in Table 2 along with expected plastic capacities calculated from theory.

Figure 3: Hollow Tube Results

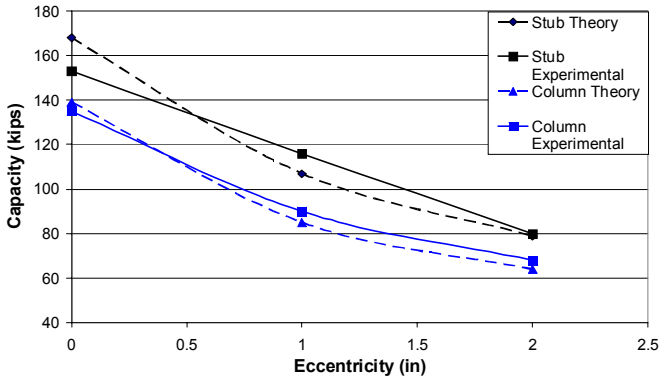


Figure 5: CFT Results

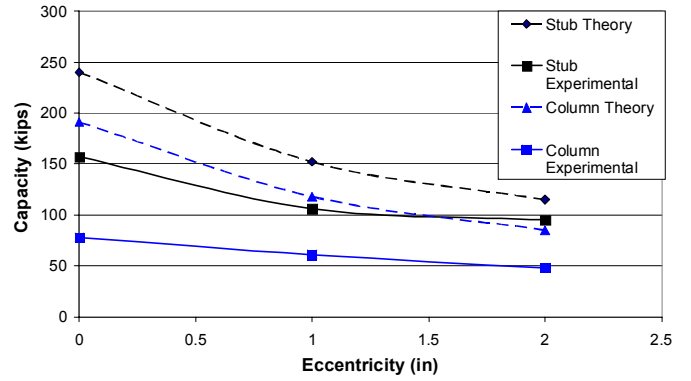


Figure 4: Local Buckling of Hollow Tube

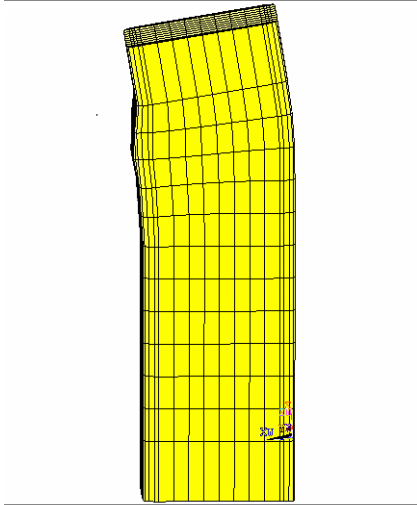
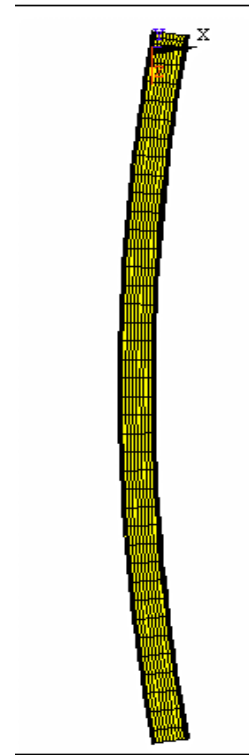


Figure 6: Global Buckling Of Hollow Tube



Inspection of the results shows that all tests failed to carry the expected load predicted by theory. Figure 5 plots the results for the CFT specimens. The graph shows that the error is greatest for smaller values of eccentricity and that the slender columns carried less percentage of load than the stub columns. These results shown that the CFT models are not producing accurate results. Possible reasons for this will be discussed further in the further research section of this article.

Table 2: CFT Results

e (in)	CFT Stubs		CFT Columns	
	Theory	ANSYS	Theory	ANSYS
0	168	153	139	135
1	107	116	85	90
2	79	80	64	68

While the capacities of the specimens are not correct, Figure 5 shows the decrease in capacity caused by increased eccentricity.

Figure 6 shows the deflected shape of the CFT column at failure. As expected the failure can be defined as global buckling of the section. Inspection of the stress distribution at failure showed that the steel tube had not reached its yield strength at failure; therefore the failure was controlled by global instability.

Time History Analysis

The conclusions of buckling modes above were based on stress distributions and inspection of the deformed geometry.

The time history postprocessor was also used to verify the failure modes described above. Figure 7 shows the load-deflection curve for a node located at the location of local buckling on the hollow stub tube shown in Figure 4. The graph is a clear case of buckling failure, where the load deflection curve bifurcates suddenly at a given value of load. We would also expect that the stress at the localized region of buckling would begin dropping load at the same load as the bifurcation point was reached in the load-deflection curve. Figure 8 shows the load-stress plot for the same node plotted in Figure 7. As expected we see that at a given value of load, the material in that region is carrying less load. This agrees with the fact that local buckling is characterized by localized yielding of the section.

Figure 7: Load-Deflection at Localized Buckling

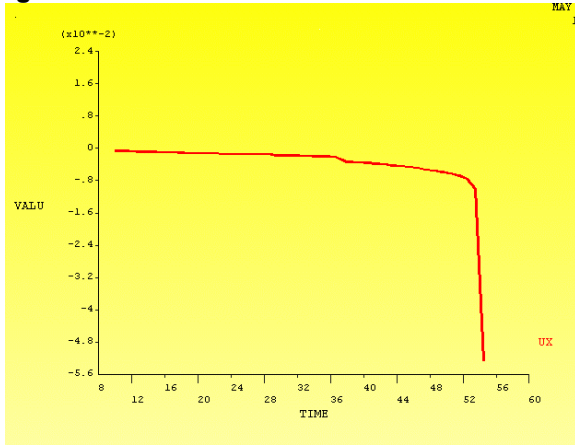
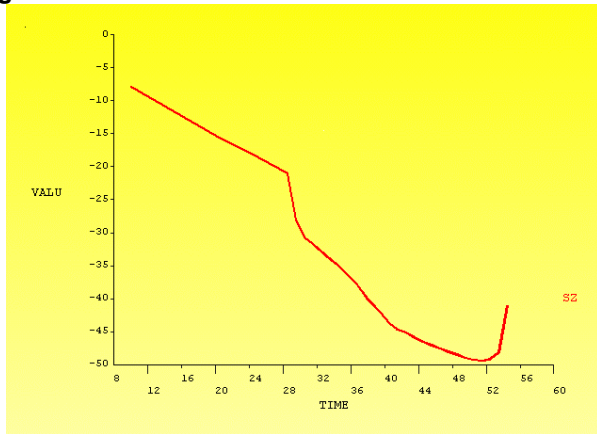


Figure 8: Load- Vertical Stress at Localized Buckling



Stress Distribution

One focus of this study was to analyze the stress distributions within the section at failure. Both vertical and cross-sectional stress distribution were looked at. Stress distributions were of interested in order to better understand the behavior of the column under loading. The stress profiles for the hollow tube section that is shown in Figure 4, show large

stress concentrations around the region of buckling. This shows that as local buckling occurs, stress is redistributed around the material that has deflected out of plane. Figure 9 shows a plot of the vertical stress profile for the hollow stub section.

For the slender column shown in Figure 6 the stress profile is uniform over the length of the tube. The distribution of vertical stresses is shown in Figure 10 for the slender column. Observation of the stresses shows that the stress profile is largely due to the bending imposed by the eccentric loading. We can see distinctly that one side of the tube is experiencing large compressive forces, while the other is almost going into tension.

Figure 9: Vertical Stresses in Hollow Stub

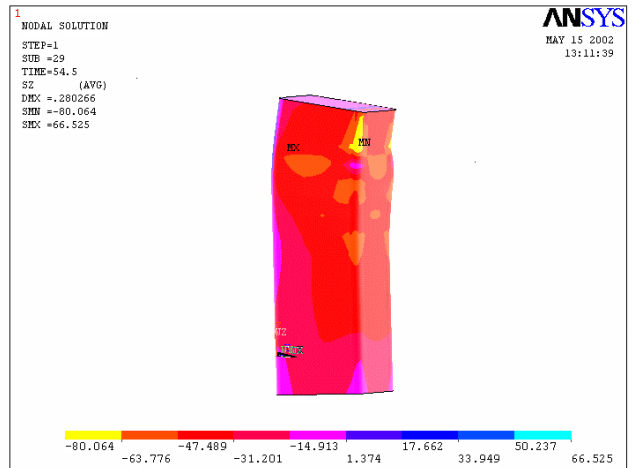
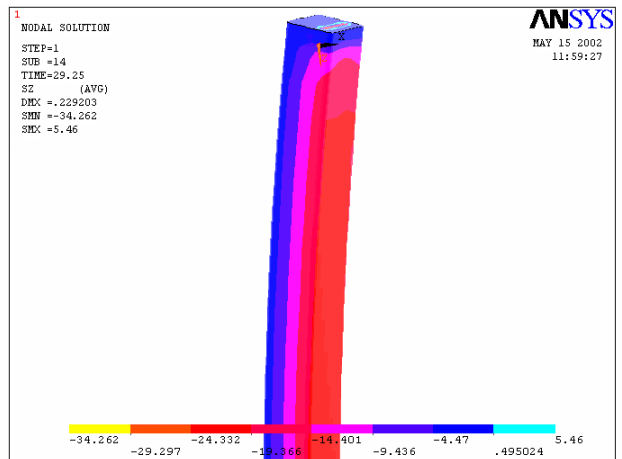


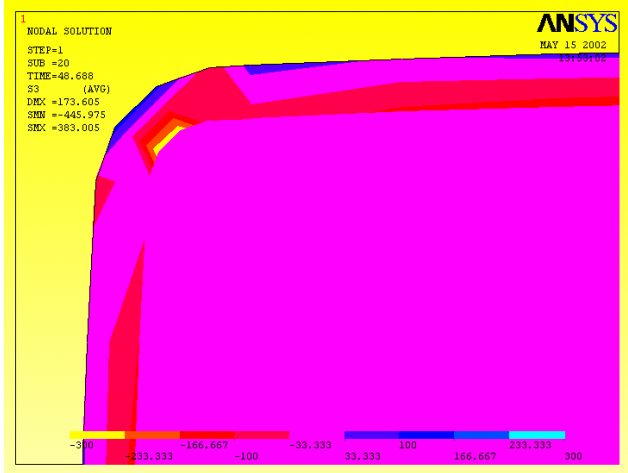
Figure 10: Vertical Stresses in CFT Stub



Also of interest in the study was the stress distribution through cross-section of the CFT columns. Figure 11 shows a plot of the in-plane stresses of the CFT stub column under concentric load. This figure shows that stress concentrations exist in the steel tube, at the corner. This result was also expected due to the fact that the corners of the steel tube are more effective in resisting the confining stresses of the concrete.

As the concrete tries to expand due to Poisson's effect, it applies a lateral force to the steel tube. This lateral force causes flexure of the faces of the steel tube; this bulging of the tube can be seen in Figure 11.

Figure 11: Cross-Sectional Stress Distribution



CONCLUSION

The expected modes of buckling were captured for both the hollow and CFT sections. Short column failure was characterized by localized buckling of the steel tube while failure of slender columns was governed by global buckling of the section. Comparison of the hollow and CFT stubs showed that localized crimping of the steel tube was prevented by the concrete core. This result may be erroneous due to the assumption of perfect bonding of the steel-concrete interface.

The capacities of the hollow section models match those predicted by theory. The deterioration of axial capacity with increasing load eccentricity was also captured by both the hollow and CFT models. However the capacities for the CFT models did not match those predicted by theory. It is concluded that the assumption of perfect bonding failed to accurately model the composite action between the two materials.

FURTHER RESEARCH

The models developed in this study will be used in future research to investigate the interface bond of the composite sections. Research will proceed with the use of contact elements located at the interface of the two materials. Contact elements allow the two materials to separate at a given value of stress and slide with respect to one another with a given coefficient of friction.

Once theoretical values can be matched, the effects of varying the point of load application will be studied. Models will be analyzed for loading of the steel section only, the concrete section only, and loading of the entire cross-section.

Due to limited processing capabilities, symmetry may be utilized on future models to allow for smaller element sizes

along the length of the tube. Some elements in the models used in this study violated shape warning limits. Reducing the aspect ratio of the elements may increase the accuracy of the models.

ACKNOWLEDGMENTS

A.K.

REFERENCES

LRFD: Manual of Steel Construction, AISC 1998